# RSC Advances

## PAPER

# Dual-enzyme natural motors incorporating decontamination and propulsion capabilities†

Sirilak Sattayasamitsathit,[a] Kevin Kaufmann,[a] Michael Galarnyk,[a] Rafael Vazquez-Duhalt[b] and Joseph Wang*[a]

Self-propelled dual-function biocatalytic motors, consisting of unmodified natural tissue and capable of in-motion bioremediation, are described. These enzyme-rich tissue motors rely on the catalase and peroxidase activities of their *Raphanus sativus* radish body for their propulsion and remediation actions, respectively. The continuous movement of the biocatalytic tissue motors through the contaminated sample facilitates the dynamic removal of phenolic pollutants. Hydrogen peroxide plays a dual role in the propulsion and decontamination processes, as the motor fuel and as co-substrate for the phenol transformation, respectively. Localized fluid transport and mixing, associated with the movement of the radish motors and corresponding generation of microbubbles, greatly improve the remediation efficiency resulting in maximal removal of pollutants within 3 min. The new 'on-the-fly' remediation process is cost effective as it obviates the need for expensive isolated enzymes and relies on environmental-friendly plant tissues.

## Introduction

There are major demands for the removal of toxic pollutants from environmental matrices ranging from groundwater to river water.[1,2] Bioremediation methods are based on the use of specialized bacteria, fungi, plants, as well as pure enzymes, capable of biocatalytically transforming toxic pollutants to non-toxic or less toxic compounds.[3–7] The challenges and opportunities of using isolated enzymes for large-scale environmental processes have been reviewed.[7–9] For example, peroxidases, which are widely distributed in nature, are able to oxidize a wide range of electron-donor compounds, including phenolic compounds, aromatic amines, industrial dyes, or pesticides.[10,11] Fungal peroxidases are directly involved in the degradation of various xenobiotic compounds,[12] while plant peroxidases have been proposed for the removal of phenolic compounds, leading to non-toxic reaction products.[13,14] However, the widespread use of peroxidases in bioremediation processes has been hindered by the high cost of the enzyme purification process[15] and a low operational stability.[16] Enzyme-rich plant tissues have been proposed as attractive alternatives to isolated enzymes for addressing the challenges of enzyme stability, availability and cost.[17] Such plant tissues offer attractive features for bioremediation processes owing to their high level of enzymatic activity,

high thermal stability (associated with confinement of the enzyme in its natural environment), negligible environmental impact, and extremely low costs. The application of plant tissues to the treatment of contaminated water can be performed either periodically in reactors with mechanical stirring, or continuously, using columns packed with the minced plant material.[18]

Here we demonstrate the ability to propel the remediation plant materials through the polluted sample toward improved contamination efficiency. The movement in nano- and micro-scale objects has been the subject of considerable efforts that led to different propulsion mechanisms and motor designs.[19–21] Among these, considerable attention has been given to self-propelled chemically-powered micromotors based on the catalytic decomposition of a fuel (most commonly hydrogen peroxide).[19,20,22–24] Enzyme (catalase)-based synthetic micro-engines have been introduced as alternatives to Pt-based catalytic motors.[25] Self-propelled biocatalytic plant tissue motors have been demonstrated recently,[26] but not in connection to bioremediation process.

The new 'on-the-fly' bioremediation concept relies on a dual-function tissue biomotor, coupling self propulsion through the contaminated sample with an in-motion biocatalytic remediation. As illustrated in Fig. 1, such in-motion remediation strategy is based on cherry-belle radish (*Raphanus sativus*), rich with the catalase and peroxidase enzymes, essential for the propulsion and detoxification functions, respectively. Peroxidase in Shepherd's Purse Roots was found to be an extremely efficient plant for the detoxification process.[18] The biocatalytic activity of enzymes in plant tissues may be varied; however, each

[a]*Department of Nanoengineering, University of California San Diego, La Jolla, CA 92093, USA. E-mail: josephwang@ucsd.edu*

[b]*Center for Nanosciences and Nanotechnology, UNAM, Ensenada, Baja California, Mexico*
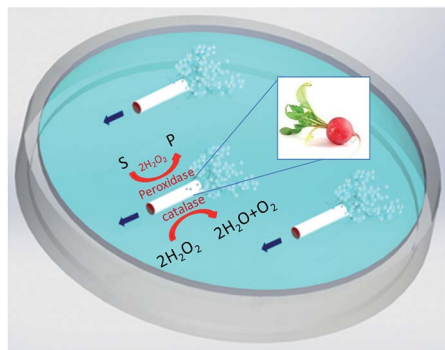
Fig. 1 Schematic illustration of the dual-function plant (radish) motors, with the catalase-driven propulsion and peroxidase-based decontamination capability, for in-motion bioremediation.

plant has numerous peroxidase isoenzymes that can be accounted for the activity up to 86% in the crude homogenate.[27] The new tissue motors thus rely on their natural catalase activity for the peroxide-driven propulsion and on their peroxidase activity for the transformation of toxic phenolic pollutants. The propulsion and remediation actions are thus carried out using the natural enzymes, hence obviating the need for expensive enzyme purification. Asymmetric biomotor design, essential for the effective catalase-driven bubble propulsion, is achieved by keeping the thick skin of the radish intact as a cap on one side of the tissue cylinder. The simultaneous propulsion/remediation operation relies on using the hydrogen peroxide not only to power the biomotor but also as a co-substrate for the peroxidase remediation reaction. The peroxidase-based biocatalytic decontamination process is thus carried out 'on-the-fly' while moving the motors continuously through the contaminated water systems. The movement of such tissue motors and the extensive generation of oxygen microbubbles induce fluid transport and "self-stirring" that accelerates the peroxidase-based decontamination process. Motion-induced convection leading to faster environmental remediation has been recently demonstrated in connection to self-propelled artificial micromotors.[28–30] Compared to nano/microscale motors, the present millimeter-size 'large' motors can reach large areas of a contaminated sample. At the end of this work we have demonstrated the immobilization of external catalase onto the plant motors to lower the peroxide fuel concentration and improve the propulsion force, towards enhanced bioremediation activity of the tissue peroxidase.

## Results and discussion

The new tissue-motor bioremediation concept has been demonstrated using peroxidase and catalase-based oxidation of phenolic contaminants and hydrogen peroxide. Phenolic compounds and their derivatives are a major class of pollutants in wastewater resulting from industrial effluents, including petroleum, coal conversion, resins, textile dyes and paper processing.[31] Such compounds represent a public health risk and are heavily regulated in many countries, and must be removed

from wastewater so they are not discharged into the environment.[7] For example, phenol, 2-chlorophenol, and 2,4-dichlorophenol are ranked within the 250 most hazardous pollutants[32] and can accumulate in the food chain. Phenolic compounds are widely spread in the environment due to industrial pollution. The World Health Organization has limited phenol concentration in drinking water to 1 μg L$^{-1}$, while a typical wastewaters from oil refineries contain phenol in concentrations ranging from 500 to 1500 mg L$^{-1}$.[33] Conventional biological wastewater treatments of polluted waters containing high phenol content are not feasible owing to the phenol toxicity towards the microorganisms.[34] In contrast, the enzymatic removal of phenols from highly polluted waters is a viable bioremediation option.

Fig. 2 displays optical images (top) and UV-Vis absorption spectra (bottom) of the reaction product of guaiacol (A), catechol (B) and 2-amino-4-chlorophenol (2A-4CP) (C) in the presence of the radish tissue biomotors. Experiments were carried out in a 1 mL solution in the absence (a) and presence (b) of 10 biomotors using a reaction time of 3 min. Both the images and the spectrophotometric data clearly indicate the formation of the reaction product in the presence of the motors, reflecting the peroxidase-based biocatalytic oxidation of guaiacol, catechol and 2A-4CP. The catalytic cycle of radish peroxidase is similar to that of other peroxidases where ferric enzyme is first oxidized by $H_2O_2$ to generate the two-electron oxidized intermediate, compound I.[35] Compound I is then reduced by one electron donated by the phenolic substrate, yielding the 1-electron oxidized enzyme intermediate, compound II, and a free radical product. The catalytic cycle is completed by the one-electron reduction of compound II by a second substrate molecule. A clear color change is thus observed in the optical images of Fig. 2, reflecting the multimeric reaction product (b). No such color change is observed without the motors (a). Similarly, well defined absorbance bands are observed in the presence of the motors at 470, 410 and 395 nm for guaiacol, catechol and 2A-4CP, respectively. In contrast, no signals are obtained in the control experiments without the biomotors (a) or with the motors but without $H_2O_2$ (not shown) over the same time.

Fig. 3A displays time-lapse images of the propulsion of the tissue motors in 5% $H_2O_2$ over a 24 s time period. As indicated
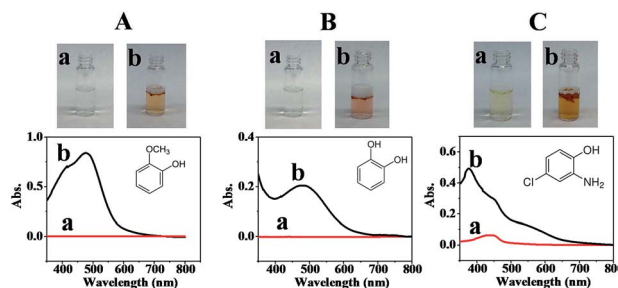


Fig. 2 UV-Vis absorption spectra (bottom) and images (top) of the product of 25 mM guaiacol (A), 25 mM catechol (B) and 2.5 mM 2A-4CP (C) obtained after a 3 min period in the absence (a) and presence (b) of the tissue motors. One mL solution containing 10 tissue motors, 5% $H_2O_2$ and 0.5% SDS.
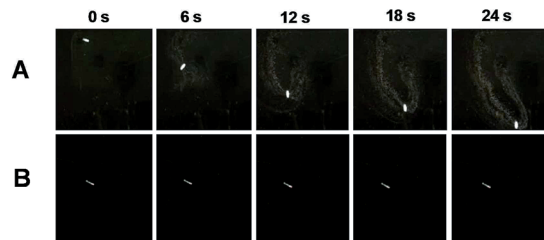
**Fig. 3** Time-lapse images of the propulsion of the plant motors in the presence (A) and absence (B) of 5% $H_2O_2$. Images taken from video ESI video 1.†

also from the corresponding ESI video 1,† immersing the tissue motor into the $H_2O_2$ solution results in a rapid bubble generation and with self propulsion of the motor at a speed of 5 mm $s^{-1}$ (or 0.6 body length per s). Intense generation of oxygen microbubbles is thus observed from most sides of the moving tissue, reflecting the very high rate of the $H_2O_2$ decomposition to water and $O_2$ (*i.e.*, catalase activity), and the asymmetric motor structure (associated with the skin cap). In contrast, no such movement and bubble generation are observed in Fig. 3B for a control experiment without the $H_2O_2$ fuel. The motor movement allows the environmentally-friendly self-propelled tissue motors to reach different areas of a contaminated sample. The lifetime of such radish-tissue biomotor was evaluated; the motors can propel up to 1 min. Bubbles still generated thereafter inducing continuous convective fluid mixing. In addition, the movement of the motor and the corresponding bubble stream enhance imparts local fluid convection and mixing of the contaminated sample, reducing mass transfer limitations during the bioremediation process.

Fig. 4 illustrates the transformation rate of guaiacol (A), catechol (B) and 2A-4CP (C) using the tissue motors and different concentrations of the pollutant. Fitting the data in a Michaelis–Menten kinetic equation, the corresponding Michaelis–Menten constant ($K_M$) of these pollutants were 33.7, 76.8 and 5.6 mM for guaiacol, catechol and 2A-4CP, respectively. The maximum transformation rates ($V_{max}$) for guaiacol (A), catechol (B) and 2A-4CP (C) using natural motors are 3.4 ± 0.6, 25.6 ± 1.5, and 3.0 ± 0.2 mg $L^{-1}$ $min^{-1}$, respectively, for a motor density of 10 motors per mL. These results indicate that the treatment of common municipal and oil-refinery wastewaters containing around 1 to 600 mg $L^{-1}$ of phenols would require between 1 and 4 tissue motors per mL, respectively, for a complete removal of the phenol within 1 hour.
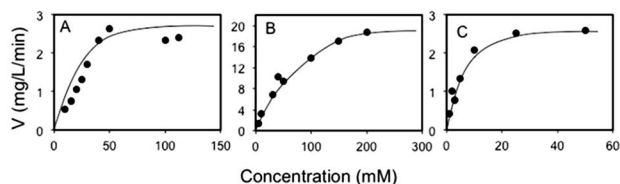
Hydrogen peroxide serves both as the fuel for the catalase-driven motion and as co-substrate for the peroxidase decontamination reaction, *i.e.*, both enzymes compete for the same peroxide substrate. In view of such dual use, the effect of the $H_2O_2$ concentration upon the transformation rate of phenolic compounds has thus been examined. As illustrated in Fig. 5, increasing the $H_2O_2$ concentrations from 1% to 10% (a–c) lowers the transformation rates of both guaiacol (A) and catechol (B). High concentration of $H_2O_2$ is generally harmful for enzymes,[36] and such trend reflects the inactivation of peroxidase at the high peroxide levels,[16,36] a 5% $H_2O_2$ concentration was used here to meet the propulsion requirement (as no movement was observed at 1% $H_2O_2$) and for enhancing the remediation. When exposed to such high levels of $H_2O_2$, peroxidases exhibit a kinetic behaviour called "suicide inactivation", in which hydrogen peroxide reacts with the catalytic intermediate compound II to form a highly reactive peroxyiron(III)porphyrin free-radical called compound III. This compound III is not part of the peroxidase cycle, but is reactive enough that is able to self-oxidize its heme active site or any other amino acid of the protein, leading to an inactive form of the enzyme. As indicated from Fig. 5, such inactivation of the plant peroxidase plays a major role in the observed dependence on the peroxide level, compared to the peroxide effect upon the phenol transformation and propulsion processes (where increasing peroxide levels are expected to offer improved removal).

In order to reduce $H_2O_2$ concentration and enhance the peroxidase activity of the natural motors, we examined the immobilization of exogenous catalase to the radish motors in a manner illustrated in the scheme of Fig. 6a. Such confinement of isolated catalase onto the end of the cylindrical radish motor greatly reduces the required fuel concentration to 0.01% (compared to 5% $H_2O_2$, generally use to propel motors), and hence minimizes the peroxidase inactivation process. Fig. 6b–d illustrates the trajectory of catalase-modified tissue motors in different $H_2O_2$ concentrations ranging from 0.01 to 0.1% (takes from ESI video 2†). Motor speeds of 14, 20 and 17 mm $s^{-1}$ are estimated in (b) 0.01%, (c) 0.05%, (d) 0.1% $H_2O_2$, respectively, corresponding to 2.8, 4.0 and 3.4 bl $s^{-1}$. This data indicates that the tissue-enzyme hybrid motors propel efficiently over large areas using low peroxide fuel levels. Such propulsion is expected to depend on the external catalase activity, immobilized in agarose gel, which improves the biomotor performance.[37] No



**Fig. 4** Transformation rate of guaiacol (A), catechol (B) and 2A-4CP (C) using tissue motors. Solution contains 10 biomotors per mL, 5% $H_2O_2$, 0.5% SDS and reaction time of 3 min (A and B) and 4 min (C).
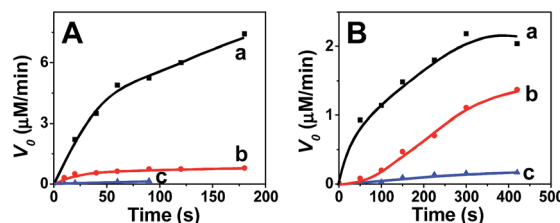


**Fig. 5** Decontamination efficiency of 25 mM guaiacol (A) and catechol (B) using natural motors in different peroxide concentrations (a) 1%, (b) 5% and (c) 10% $H_2O_2$.
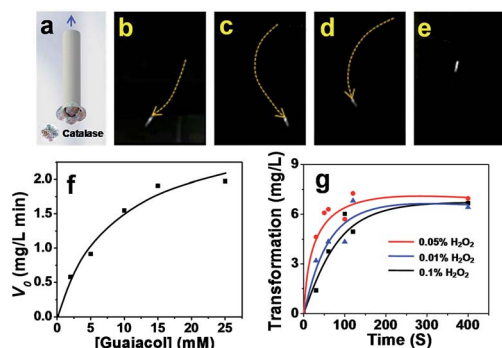
Fig. 6 (a) Schematic of the natural motors with external catalase (a) and (b–e) time-lapse images of the propulsion of these tissue-enzyme hybrid motors (with exogenous catalase) over 2 s in the presence of (b) 0.01%, (c) 0.05%, (d) 0.1% $H_2O_2$ and (e) without $H_2O_2$. The catalase was attached to the end of the radish motor by confining catalase-coated agarose beads. (f) Michaelis–Menten plot for guaiacol in the presence of 0.1% $H_2O_2$ and (g) transformation rate of guaiacol in different hydrogen $H_2O_2$ concentrations. Motor density, 1 motor per mL. Track lines b–d were taken from video ESI video 2.†

apparent movement is observed in Fig. 6e in a control experiment carried out in a 0.1% $H_2O_2$ solution without the exogenous catalase. Fig. 6f illustrates that the hybrid tissue-enzyme motors display a Michaelis–Menten behaviour for guaiacol in the presence of 0.1% $H_2O_2$ and varying guaiacol concentrations (0–25 mM). The corresponding $K_M$ and $V_{max}$ for guaiacol are 8.2 mM and 2.7 mg L$^{-1}$ min$^{-1}$, respectively, for a motor density of 1 motor per mL. These values compare favourably with $K_M$ and $V_{max}$ values determined from the data in Fig. 4 for the radish motors (without the exogenous catalase). Fig. 6g shows the transformation rate for guaiacol observed for the hybrid tissue-enzyme motor using different $H_2O_2$ concentrations ranging from 0.01 to 0.1%. The highest initial transformation rate is observed using 0.05% (16 mM) $H_2O_2$. Generally, the maximum catalytic activity of plant peroxidase is achieved at millimolar $H_2O_2$ concentrations.[38] Our experiment requires a higher $H_2O_2$ concentration for implementing the simultaneous propulsion task. However, the attached external catalase can dramatically (100-fold) lowers the required peroxide fuel concentration and leads to a 8-fold enhanced decontamination efficiency, but increases the cost of the motor and its preparation time.

The improved decontamination rate in the presence of exogenous catalase reflects the greatly higher peroxidase activity as well as the enhanced motor speed and corresponding convective fluid transport. The lifetime and speed of the radish-tissue biomotor, with the exogenous catalase, were evaluated in a 0.1% $H_2O_2$ solution (ESI video 3†). The natural motors displayed lifetimes approaching 3 min, with a gradual decrease of their speed from 28 to 5 mm s$^{-1}$; such speed diminution depended on the $H_2O_2$ concentration.

The proof of concept for biocatalytic plant-tissue biomotors has been demonstrated. Besides that the key point of using extremely low-cost and fully-natural biomotors, it is possible to improve the performance, especially the lifetime, by co-immobilization of a peroxide-generating oxidase enzyme (e.g., glucose- or alcohol-oxidases), to obtain a self-sufficient

biomotor without the need of exogenous peroxide.[39] In addition, new catalytic activities could be obtained by using other plant tissues with a specific activity or by the immobilization of another enzyme.

## Experimental

### Tissue biomotors preparation

Tissue motors were prepared by cutting 7 mm thick slices of radish containing skin on the outside. Small cylindrical motors were punched out of the plant cross section using a 1.0 mm-diameter Harris puncher (Redding, CA) with length of 7 mm. One end of the resulting rod was capped with the red skin of the radish to create an asymmetric structure. The asymmetric bubble propulsion forces resulted from the catalase oxidized $H_2O_2$ generating $O_2$ bubbles. Multiple motors prepared from the same section or from different radish plants displayed 5 to 8% changes in the observed contamination efficiency, reflecting variations in the levels of the two enzymes. For the catalase-modified tissue motors, the skin end was coated with catalase, immobilized on agarose beads (Sigma-Aldrich) using a cyano-acrylate glue (Krazy Glue). Such modification of the tissue cylinder with catalase immobilized on agarose beads allows the motors to generate $O_2$ bubbles and propel at low $H_2O_2$ concentration.

### Tissue motor propulsion

The hydrogen peroxide solutions, used as a fuel for tissue motor propulsion, also contained 0.5% (w/v) sodium dodecyl sulfate (SDS). The autonomous propulsion of the tissue motors (associated with the asymmetric structure caused by the presence of the radish skin on one end of the motor) was tested in various $H_2O_2$ concentrations (1%, 5%, and 10%). The propulsion of the external catalase modified tissue motors, prepared by attaching catalase-encapsulated in agarose beads, was tested in 0.01, 0.05, 0.1 and 1% $H_2O_2$ concentrations. The increase in catalase activity allowed the motors to move autonomously in these low concentrations of $H_2O_2$. The bubble generation and movement of the tissue motors were recorded using an iPhone 4S camera.

### Peroxidase activity

Absorption spectra were collected with a spectrophotometer (UV2450, Shimadzu) with 1 cm path-length cells. The absorbance of the 600 μL samples was measured over the 300–800 range. A baseline was determined for each experiment using a blank solution of the same composition. The transformation rates were determined by monitoring the absorbance of the solution at 480 nm, 470 nm, and 395 nm for guaiacol, catechol, and 2-amino-4-chlorophenol (2A-4CP), respectively. The extinction coefficients for guaiacol ($\varepsilon_{470nm}$ = 26 600 M$^{-1}$ cm$^{-1}$),[40] catechol ($\varepsilon_{410nm}$ = 1623 M$^{-1}$ cm$^{-1}$)[41] and 2A-4CP ($\varepsilon_{395nm}$ = 21 000 M$^{-1}$ cm$^{-1}$)[42] were used. All chemicals were purchase from Sigma. Phenol transformation assays were determined by monitoring the absorbance after 3 minutes, in a solution containing different concentrations of pollutants, 10 motors, 5% $H_2O_2$, and 0.5% SDS. Pollutants concentrations

were increased until the rate remained constant even upon further increasing the concentration (substrate-saturating concentration). In case of exogenous catalase modified tissue motors, the Michaelis–Menten plot was determined in the presence of 1 motor, 0.1% $H_2O_2$ and 0.5% SDS *versus* different concentrations of guaiacol (0–25 mM).

## Conclusions

We have demonstrated a novel cost-effective biomotor strategy, based on the presence of multiple enzymes in plant tissues that combines efficient propulsion with 'on-the-fly' bioremediation. The resulting dual-function (motion/remediation) devices have been used successfully for accelerated decontamination of phenolic compounds. Such effective decontamination reflects the motor-induced fluid transport and mixing and movement over relatively large areas which add a new dimension to such remediation procedures. Such use of plant tissues offers a cost-effective bioremediation strategy as they are environment-compatible and are extremely inexpensive. These millimeter-size 'large' motors can reach large areas of a contaminated sample accelerating the decontamination process without external mixing force. Improved performance, but at a higher cost and complexity, has been achieved using hybrid tissue-enzyme motors. Current efforts are aimed at scaling up the process from the bench scale to large-volume pilot studies, at replacing the SDS surfactant with naturally-occurring surface-active materials, and at assessing the effect of the rotting plant materials upon the water samples. The concept of self-propelled decontaminating natural motors can be expanded to different tissues rich with other enzymes (*e.g.*, polyphenol oxidase), along with catalase, towards self-sustainable decontaminating natural motors.

## Acknowledgements

## Notes and references

1  F. W. Whicker, T. G. Hinton, M. M. MacDonell, J. E. Pinder III and L. J. Habegger, *Science*, 2004, **303**, 1615.

2  L. W. Perelo, *J. Hazard. Mater.*, 2010, **177**, 81.

3  M. Megharaj, B. Ramakrishnan, K. Venkateswarlu, N. Sethunathan and R. Naidu, *Environ. Int.*, 2011, **37**, 1362.

4  S. Rayu, D. G. Karpouzas and B. K. Singh, *Biodegradation*, 2012, **23**, 917.

5  E. L. Rylott, A. Lorenz and N. C. Bruce, *Curr. Opin. Biotechnol.*, 2011, **22**, 434.

6  T. Kudanga, S. Burton, G. S. Nyanhongo and G. M. Guebitz, *Front. Biosci.*, 2012, **4**, 1127.

7  J. Karam and J. A. Nicell, *J. Chem. Technol. Biotechnol.*, 1997, **69**, 141.

8  M. Ayala, M. A. Pickard and R. Vazquez-Duhalt, *J. Mol. Microbiol. Biotechnol.*, 2008, **15**, 172.

9  H. Qayyum, H. Maroof and K. Yasha, *Crit. Rev. Biotechnol.*, 2009, **29**, 94.

10 R. E. Parales and J. D. Haddock, *Curr. Opin. Biotechnol.*, 2004, **15**, 374.

11 C. Torres-Duarte and R. Vazquez-Duhalt, in *Biocatalysis Based on Heme Peroxidases: Peroxidases as Potential Industrial Biocatalysts*, ed. E. Torres and M. Ayala, Springer, Heidelberg, 2010, pp. 179–206.

12 N. Magan, S. Fragoeiro and C. Bastos, *Mycobiology*, 2010, **38**, 238.

13 F. Quintanilla-Guerrero, M. A. Duarte-Vázquez, B. E. García-Almendarez, R. Tinoco, R. Vazquez-Duhalt and C. Regalado, *Bioresour. Technol.*, 2008, **99**, 8605.

14 M. F. Máximo, M. Gómez, M. D. Murcia, S. Ortega, D. S. Barbosa and G. Vayá, *Environ. Technol.*, 2012, **33**, 1071.

15 E. E. Hood, *Enzyme Microb. Technol.*, 2002, **30**, 279.

16 B. Valderrama, M. Ayala and R. Vazquez-Duhalt, *Chem. Biol.*, 2002, **9**, 555.

17 J. Wang and M. S. Lin, *Anal. Chem.*, 1988, **60**, 1545.

18 J. W. Park, B. K. Park and J. E. Kim, *Arch. Environ. Contam. Toxicol.*, 2006, **50**, 191.

19 J. Wang, *Nanomachines: Fundamentals and Applications*, Wiley-VCH, Weinheim, 2013, ISBN 978-3-527-33120-8.

20 J. Wang and W. Gao, *ACS Nano*, 2012, **6**, 5745.

21 W. Gao, S. Sattayasamitsathit, K. M. Manesh, D. Weihs and J. Wang, *J. Am. Chem. Soc.*, 2010, **132**, 14403; G. Loget and A. Kuhn, *J. Am. Chem. Soc.*, 2010, **132**, 15918.

22 M. Pumera, *Nanoscale*, 2010, **2**, 1643; T. E. Mallouk and A. Sen, *Sci. Am.*, 2009, **300**, 72.

23 W. Gao, S. Sattayasamitsathit, A. Uygun, A. Pei, A. Ponedal and J. Wang, *Nanoscale*, 2012, **4**, 2447.

24 Y. Mei, A. A. Solovev, S. Sanchez and O. G. Schmidt, *Chem. Soc. Rev.*, 2011, **40**, 2109.

25 S. Sanchez, A. A. Solovev, Y. Mei and O. G. Schmidt, *J. Am. Chem. Soc.*, 2010, **132**, 13144; J. Orozco, V. Garcia-Gradilla, M. D'Agostino, A. Cortes and J. Wang, *ACS Nano*, 2013, **7**, 818.

26 Y. Gu, S. Sattayasamitsathit, K. Kaufmann, R. Vazquez-Duhalt, W. Gao, C. Wang and J. Wang, *Chem. Commun.*, 2013, **49**, 7307.

27 L. M. Shannon, K. Ernest and J. Y. Lew, *J. Biol. Chem.*, 1966, **241**, 2166.

28 J. Orozco, G. Cheng, D. Vilela, S. Sattayasamitsathit, R. Vazquez-Duhalt, G. Valdés-Ramírez, O. S. Pak, A. Escarpa, C. Kan and J. Wang, *Angew. Chem., Int. Ed.*, 2013, **52**, 13276.

29 L. Soler, V. Magdanz, V. M. Fomin, S. Sanchez and O. G. Schmidt, *ACS Nano*, 2013, **7**, 9611.

30 G. Zhao, E. J. Stuart and M. Pumera, *Phys. Chem. Chem. Phys.*, 2011, **13**, 12755.

31 A. Kumar, S. Kumar and S. Kumar, *Biochem. Eng. J.*, 2005, **22**, 151.

32 EPA, 2013, US Environmental Protection Agency, Superfund national priorities list for remediation, 40 CFR 423, A Code of Federal Regulations.

33 R. E. Kirk and D. F. Othmer, *Encyclopedia of chemical toxicology*, NY, 3rd edn, 1980.

34 A. Uygur and F. Kargi, *Process Biochem.*, 2004, **39**, 2123.

35 P. R. Ortiz de Monetllano, in *Biocatalysis Based on Heme Peroxidases: Peroxidases as Potential Industrial Biocatalysts*, ed. E. Torres and M. Ayala, Springer, Heidelberg, 2010, pp. 79–110.

36 K. Hernandez, A. Berenguer-Murcia, R. C. Rodrigues and R. Fernandez-Lafuente, *Curr. Org. Chem.*, 2012, **16**, 2652.

37 C. Garcia-Galan, A. Berenguer-Murcia, R. Fernandez-Lafuente and R. C. Rodrigues, *Adv. Synth. Catal.*, 2011, **353**, 2885.

38 H. Garcia-Arellano, in *Biocatalysis Based on Heme Peroxidases: Peroxidases as Potential Industrial Biocatalysts*, ed. E. Torres and M. Ayala, Springer, Heidelberg, 2010, pp. 335–352.

39 F. van de Velde, N. D. Lourenço, M. Bakker, F. van Rantwijk and R. A. Sheldon, *Biotechnol. Bioeng.*, 2000, **69**, 286.

40 R. S. Koduri and M. Tien, *J. Biol. Chem.*, 1995, **270**, 22254.

41 J. L. Muñoz, F. García-Molina, R. Varón, J. N. Rodriguez-Lopez, F. García-Cánovas and J. Tudela, *Anal. Biochem.*, 2006, **351**, 128.

42 E. Katsivela, V. Wray, D. H. Pieper and R.-M. Wittich, *Appl. Environ. Microbiol.*, 1999, **65**, 1405.